# UNCLASSIFIED

## AD 464375

DEFENSE DOCUMENTATION CENTER

FOR

SCIENTIFIC AND TECHNICAL INFORMATION

CAMERON STATION  ALEXANDRIA, VIRGINIA

# UNCLASSIFIED

# THE
# ANTENNA
# LABORATORY

## RESEARCH ACTIVITIES in ---

*Automatic Controls*    *Antennas*    *Echo Area Studies*
*Microwave Circuits*    *Astronautics*    *E M Field Theory*
*Terrain Investigations*    *Radomes*    *Systems Analysis*
*Wave Propagation*             *Submillimeter Applications*

A Servo-Controlled Nulling System
for Reducing Radio Frequency
Interference

by

James T. Campbell

Contract N123(953)-31663A

1522-5                 23 August 1963

Prepared for
U.S. Navy Purchasing Office
Los Angeles 55, California

## Department of ELECTRICAL ENGINEERING

# THE OHIO STATE UNIVERSITY
# RESEARCH FOUNDATION
Columbus , Ohio

NOTICES

When Government drawings, specifications, or other data are used for any purpose other than in connection with a definitely related Government procurement operation, the United States Government thereby incurs no responsibility nor any obligation whatsoever, and the fact that the Government may have formulated, furnished, or in any way supplied the said drawings, specifications, or other data, is not to be regarded by implication or otherwise as in any manner licensing the holder or any other person or corporation, or conveying any rights or permission to manufacture, use, or sell any patented invention that may in any way be related thereto.

The Government has the right to reproduce, use, and distribute this report for governmental purposes in accordance with the contract under which the report was produced. To protect the proprietary interests of the contractor and to avoid jeopardy of its obligations to the Government, the report may not be released for non-governmental use such as might constitute general publication without the express prior consent of The Ohio State University Research Foundation.

Qualified requesters may obtain copies of this report from the Defense Documentation Center, Cameron Station, Alexandria, Virginia. Department of Defense contractors must be established for DDC services, or have their "need-to-know" certified by the cognizant military agency of their project or contract.

# R E P O R T

by

THE OHIO STATE UNIVERSITY RESEARCH FOUNDATION
COLUMBUS, OHIO 43212

| | |
|---|---|
| Sponsor | U. S. Navy Purchasing Office<br>929 South Broadway<br>Box 5090 Metropolitan Station<br>Los Angeles 55, California |
| Contract Number | N123(953)-31663A |
| Investigation of | Study Program Related to Shipboard<br>Antenna System Environment |
| Subject of Report | A Servo-Controlled Nulling System<br>for Reducing Radio Frequency<br>Interference |
| Submitted by | James T. Campbell<br>Antenna Laboratory<br>Department of Electrical Engineering |
| Date | 23 August 1963 |

The material contained in this report is also used as a thesis
submitted to the Department of Electrical Engineering, The
Ohio State University, as partial fulfillment for the degree
Master of Science.

# ABSTRACT

The servo controlled nulling system is analyzed to determine its feasibility as a method of reducing radio frequency interference caused by nearby transmitters. Limitations on the practical form of the system are studied. Experimentation includes the measurement of null depths for low-level interfering signals.

CONTENTS

# CHAPTER I
## INTRODUCTION

Naval shipboard communication systems have always been afflicted with the problem of radio frequency interference between receivers and transmitters located on the same ship. In recent years the problem has been intensified by the introduction of more sensitive receivers and more powerful transmitters. Spacing between receiver and transmitter antennas is limited by the physical size of the ship. Solution to the interference problem is further complicated by the broad-band, omnidirectional properties of the antennas.

Measurements indicate that interfering signals with power levels in excess of several hundred watts may be present at the output terminals of the receiver antenna. The desired signal arriving from a distant source is often only microwatts in power.

Cross-modulation, a common severe form of interference, is caused by strong signals which are "off-frequency", or outside the receiver pass band. The interfering "off-frequency " signal and the weak desired signal pass through a radio frequency amplifier and mixer in a receiver such as the one illustrated in Fig. 1. Because the interfering signal is "off-frequency", it does not pass through the narrow-band intermediate-frequency amplifiers. Since the

1

Fig. 1. Block diagram of a communications receiver.

automatic gain control detector responds only to the weak desired

signal present at the intermediate-frequency output stage, the gain

of the receiver is not reduced by the interfering signal.[1] For in-

creasingly large input signals the mixer tube and eventually the radio

frequency amplifier tube become overloaded. When overloaded, the

gain curve of the radio frequency amplifier and mixer tubes in-

troduces a third-order non-linearity into the output signal. The non-

linear term causes modulation components of the interfering signal to

appear in combination with the desired signal.[2] Therefore, a

communications receiver is vulnerable to "off-frequency"

2

interference, even though it may have excellent rejection in the intermediate and audio-frequency stages.

The susceptibility of a commercial communications receiver to cross-modulation has been measured.[3] From these measurements the amount of attenuation of the interfering signal needed between the antenna output terminals and the receiver input terminals can be computed. For such a computation, the assumed conditions may be as follows: A desired amplitude-modulated signal of strength 10 $\mu$v and of frequency 4.0 mc is to be received. An amplitude modulated interfering signal of strength 100 volts and frequency 4.1 mc is also present at the receiver antenna output terminals. The desired signal is to be received with less than 10% distortion due to cross-modulation. With these conditions satisfied, the amount of additional attenuation needed at the interfering signal frequency is found to be greater than 40 db. With the advent of transistorized "front-ends", receiver susceptibility to cross-modulation has become an even greater problem.[4]

To eliminate cross-modulation, the interfering signal must be attenuated before it enters the first active element in a receiver. Passive pre-selector circuits were investigated as a means of producing the needed selective attenuation.[5] A bridged-T infinite-notch filter was constructed with a center frequency of 3.6 mc.

Measurements indicated a null depth of 70 db at the center frequency. The depth of null 10 kc away from the center frequency was 30 db. The rapid decrease of null depth with frequency deviation is due to the single-frequency nature of the notch filter. The notch filter was extremely difficult to tune to a given frequency. Because of component changes with temperature, the null frequency often drifted several kc. Mechanical vibrations, such as those occurring on board ship, also adversely affected the frequency stability of the filter.

Another method of interference suppression is signal cancellation. In the cancellation method the signal is tapped from the interfering transmitter. Given the proper amount of attenuation and time delay, the tapped signal is subtracted from the signal already present on the receiver antenna. The desired signal is not cancelled, since it is present only at the antenna output and not at the output of the processing path. A block diagram of the cancellation system, Fig. 2 in Chapter II.A., illustrates the radiated and processing paths of the interfering signal.

The cancellation technique was utilized in the suppression of periodic-pulse interference at audio frequencies in an investigation by the Georgia Institute of Technology Engineering Experiment Station.[6] Two parallel paths in the audio output circuit of a receiver are combined to provide a cancellation point. One path transfers

the audio signal, including the pulse interference, to the cancellation point. The other path synthesizes the interfering pulse and delays it to cancel the succeeding pulse in the periodic chain of pulses. The required time delay is achieved by a succession of one-shot multivibrators. The cancellation system reduced interference from the pulses by 30 db.

The interference suppression system designed at the Ohio State University Antenna Laboratory is a servo-controlled nulling system which achieves interfering-signal cancellation automatically. This method of suppressing an interfering signal is adaptable to a shipboard environment. The system automatically adjusts to changes in frequency, amplitude, and phase experienced by the interfering signal. Because of the automatic correctional nature of the system, variations in components internal to the system do not affect the null depth.

Recently the Antenna Laboratory and the author learned of a signal cancellation system being developed by Scanwell Laboratories Incorporated. According to available information, the Scanwell nulling system functions similarly to the nulling loop investigated at the Antenna Laboratory.[7] Detailed information on the Scanwell nulling system has not yet been published.

5

The following study establishes the feasibility of the servo-controlled nulling system as a technique for reducing extreme radio frequency interference between a transmitter and receiver in proximity to each other.

# ANALYSIS OF THE SERVO-CONTROLLED NULLING SYSTEM

## A. The Ideal Cancellation System

Strong signal interference from a local transmitter may be minimized by cancellation. A block diagram of an ideal cancellation system is shown in Fig. 2. The signal fed through the processing path is delayed and attenuated so that it is identical to the interfering signal present on the receiver antenna. Inverted at the summing point, the processed signal cancels the interfering signal on the receiver antenna. The properties of the ideal cancellation system are derived using Fourier transform analysis.
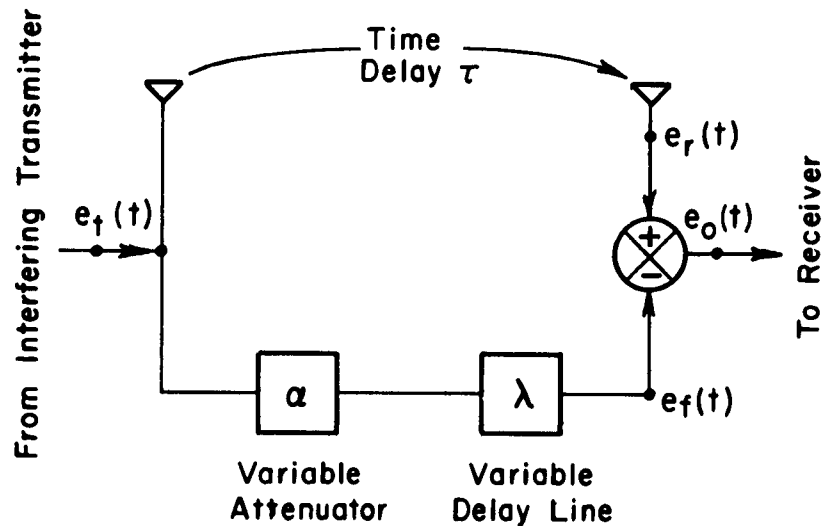
Fig. 2. Block diagram of the ideal cancellation system.

As illustrated in Fig. 2, the interfering transmitter signal is denoted by $e_t(t)$. The interfering signal on the receiver antenna is

(1) $\qquad e_i(t) = ke_t(t-\tau)$

where

$\qquad$ k = the amplitude of the interfering signal

$\qquad \tau$ = the time delay between the antennas.

As expressed in Eq. (1), the intercepted interfering signal $e_i(t)$ is assumed to be an undistorted replica of $e_t(t)$. When converted to transform notation, Eq. (1) becomes

(2) $\qquad E_i(\omega) = kE_t(\omega)\, e^{-j\omega\tau}$ .

The signal fed through the processing path, $e_f(t)$, is also an undistorted replica of $e_t(t)$ and may be written in transform notation as

(3) $\qquad E_f(\omega) = \alpha\, E_t(\omega)\, e^{-j(\omega\lambda)}$

where

$\qquad \alpha$ = the gain constant of the attenuator

$\qquad \lambda$ = the time delay in the processing path .

The signals $E_f(\omega)$ and $E_i(\omega)$, are summed at the receiver input in Fig. 2 to form $E_c(\omega)$. The resulting signal at the receiver input is expressed as

8

(4)     $E_o(\omega) = E_f(\omega) - E_i(\omega)$

(5)     $= E_t(\omega) \left[ ke^{-j\omega\tau} - \alpha e^{-j\omega\lambda} \right]$ .

For cancellation to occur, $E_o(\omega)$ must equal zero. $E_o(\omega)$ equals zero
for $\alpha = k$ and $\lambda = \tau$. With $\alpha$ and $\lambda$ equalling $k$ and $\tau$ respectively,
Eq. (5) becomes

(6)     $E_o(\omega) \Big|_{\substack{\alpha = k \\ \lambda = \tau}} = kE_t(\omega) \left[ 0 \right] = 0$ .

As indicated in Eq. (6), the fed-through signal must undergo attenuation
and time delay identical to that experienced by the interfering signal.
Furthermore, the fed-through signal must be inverted at the summing
point.

When the conditions for cancellation are satisfied, the resulting
null is infinitely deep and independent of the nature of $e_t(t)$. The
null depth independence of $e_t(t)$ is indicated in Eq. (6), in which the
cancellation conditions do not involve the signal $E_t(\omega)$. Therefore,
$E_t(\omega)$ may have a broad spectrum of frequencies and still be com-
pletely cancelled at the receiver input.

Another desirable feature of the ideal cancellation system is
that the null depth is independent of the time delay experienced by
the interfering signal. In contrast, the amount of time delay places an
important restriction on the practical system described in the next
section.

9

B. Limitations of a Variable Phase Shifter
   Nulling System

The variable delay line of the cancellation system in Fig. 2

must correct for minute variations in $\tau$. The corrections are

necessary to maintain a deep null. Since the required continuously

variable delay line is not commercially available, it must be simulated.

A variable phase shifter and constant delay line are employed for the

purpose. The phase shifter nulling system pictured in Fig. 3 is a

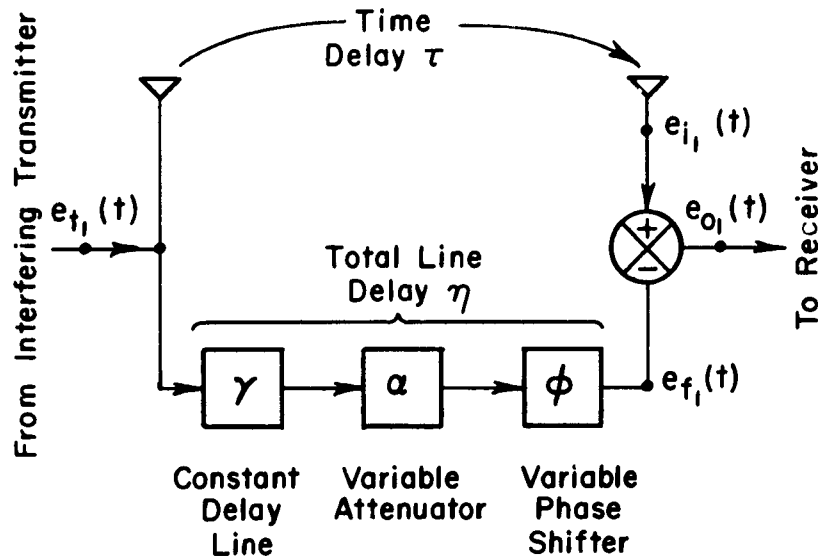practical approximation of the ideal cancellation system.



Fig. 3. Block diagram of the phase shifter nulling system.

The total constant time delay, $\eta$, of the nulling system path

in Fig. 3 is composed of a constant delay, $\gamma$, from the delay line

and the constant delay in the attenuator and phase shifter circuitry.

The time delay, $\gamma$, cannot be varied. Consequently an additional variable time delay must be added in order to follow the small deviations in $\tau$ about its mean value. The required variations in time delay are simulated by a phase shifter. The amount of phase shift, $\phi$, may be continuously varied. $\phi$ is assumed to be uniform, or constant, over a limited range of input frequencies.

The conditions for cancellation at the receiver antenna output may be determined for the phase shifter nulling system to Fig. 3. A general interfering signal $e_{i_1}(t)$ may be expressed in transform notation as

(7) $\qquad E_{i_1}(\omega) = k E_{t_1}(\omega) e^{-j\omega\tau}$

where

$\qquad$ k = the amplitude of the interfering signal

$\qquad \tau$ = the time delay between antennas.

The transform of $e_{f_1}(t)$, the signal fed through the processing path, is

(8) $\qquad E_{f_1}(\omega) = \alpha \, E_{t_1}(\omega) e^{-j(\omega\eta + \phi)}$

where

$\qquad \alpha$ = the gain constant of the attenuator

$\qquad \eta$ = the total constant time delay in the processing path

$\qquad \phi$ = the variable phase shift.

11

The composite interfering signal at the receiver input in

(9) $\qquad E_{O_1}(\omega) = E_{i_1} - E_{f_1}(\omega)$.

(10) $\qquad E_{O_1}(\omega) = E_{t_1}(\omega) [ ke^{-j\omega\tau} - \alpha e^{-j(\omega\eta + \phi)} ]$ .

Suppression of the interfering signal requires that

$E_{O_1}(\omega)$ equal zero. $E_{O_1}(\omega)$ equals zero when $\alpha = k$, and $\phi = \omega(\tau - \eta)$.

The solution specifies that $\phi$ increase with increasing frequency. As

previously described, $\phi$ is constant for the frequency components of the

input signal. Therefore, the cancellation can be complete only at a

single frequency.

The interference must consist of a continuous wave (c.w.) sig-

nal in order that it be completely cancelled. For an interfering signal

spectrum of finite width, the null in infinitely deep at only one fre-

quency. The phase error introduced at other frequencies limits the

amount of interference suppression. As shown in Fig. 4, the amount

of phase error at the sideband frequencies, $\omega_o \overset{+}{-} \omega_s$ is proportional to

$\Delta t = \tau - \eta$. Therefore, to insure a deep null over the entire interfering

signal spectrum, $\Delta t$ must be quite small.

To illustrate the limitations on the phase-shifter system, the

theoretical null depth will be computed for a sample case. The

following conditions are assumed: The receiver and transmitter

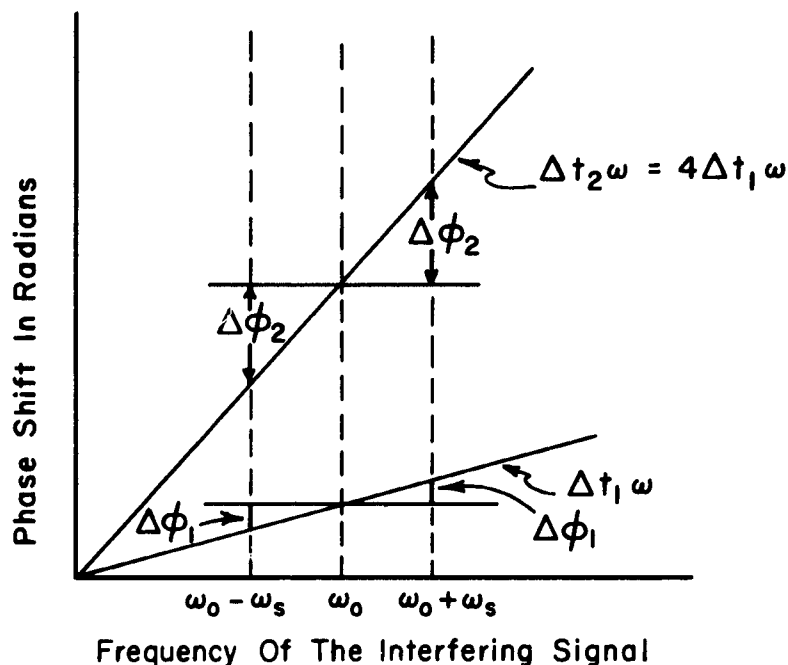units are adjacent. A distance of 30 meters exists between their

12

Fig. 4.   Phase error at sideband frequencies for the phase
shifter nulling system.

antennas.   The interfering transmitter signal has a center frequency

of 4.0 mc and sidebands at 5 kc from center frequency.   For the

assumed conditions, the processed signal time delay, $\eta$, is taken to

be zero.   The time delay, $\tau$, between antennas is $10^{-7}$ sec.   The

corresponding phase shift experienced by the delayed interfering

signal at the center frequency is

(11)        $\omega_0 \tau = 4.00 \times 6.283 \times 10^{-1} = 2.513$ radians.

13

The null-seeking servo-system, responding to the carrier signal, maintains $\phi$ at 2.513 radians. Consequently, the null is infinitely deep at the carrier frequency.

At the sideband frequencies, the null is finite in depth. The signal at the receiver input, $E_{O_1}(\omega)$ may be expressed according to Eq. (10) as

(12)
$$\left| \frac{E_{O_1}(\omega)}{kE_{t_1}(\omega)} \right| = \left| e^{-j4.005 \times 6.283 \times 10^{-1}} - e^{-j4.000 \times 6.283 \times 10^{-1}} \right|$$

(13)
$$\left| \frac{E_{O_1}(\omega)}{kE_{t_1}(\omega)} \right| = \left| e^{-j2.516} - e^{-j2.513} \right| = 2.7 \times 10^{-3}.$$

As computed from Eq. (13), the null depth at the upper side-band frequency is -51 db. Thus, the approximation of a large time delay difference, $\Delta t$, by a phase shifter imposes a significant limitation on nulling loop interference rejection.

## C. Derivation of the Error Monitoring Signals

The servo-controlled nulling system utilizes a variable phase shifter. The system is therefore subject to the limitations described in the previous section. The servo-controlled nulling system which is pictured in the block diagram of Fig. 5 is similar to the phase-shifter nulling system of Fig. 4. The main differences between the systems are the balanced modulators and servo systems which have

14

been added in Fig. 5. The balanced modulators generate sidebands which monitor the nulling error by producing phase and amplitude error signals. Servo-motors, responding to the phase and amplitude error signals, drive a phase shifter and an attenuator to the proper null position. Therefore, changes in phase or amplitude of the intercepted interfering signal are rapidly reproduced in the processing path to maintain continual cancellation of the interfering signal.

To simplify the error signal derivation, the interference is assumed to be a c.w. signal. As illustrated in Fig. 5, the interfering signal at the receiver antenna terminals is $E_a$, and the output signal of the processing path is $E_b$. When the system has achieved a null, $E_a$ and $E_b$ will be $180^\circ$ out of phase and of the same amplitude in order to cancel. However, for illustrative purposes, $E_a$ and $E_b$ are assumed to be out of phase by $180^\circ - \Delta\phi$ and to differ in amplitude by B-A. The relationship between $E_a$ and $E_b$ is shown in Fig. 6(a).

The method by which the generated sidebands monitor the phase and amplitude errors may be understood by tracing these sidebands through the nulling system illustrated in Fig. 5.

Balanced modulator I, with a signal of audio frequency $f_1$, produces sidebands which monitor the phase error, $\Delta\phi$. A constant portion of $E_g$, the signal tapped from the transmitter, is shifted $90^\circ$ in phase and introduced into balanced modulator I. As illustrated in
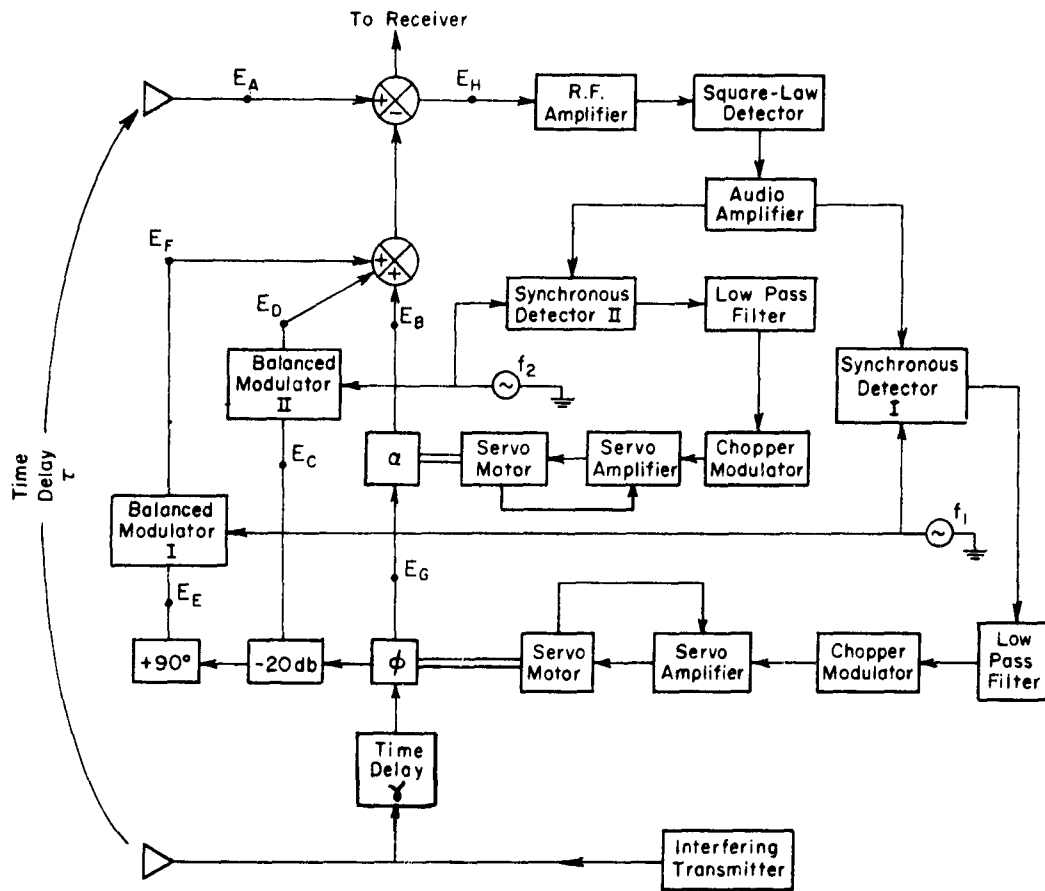
15

Fig. 5. Block diagram of the servo-controlled
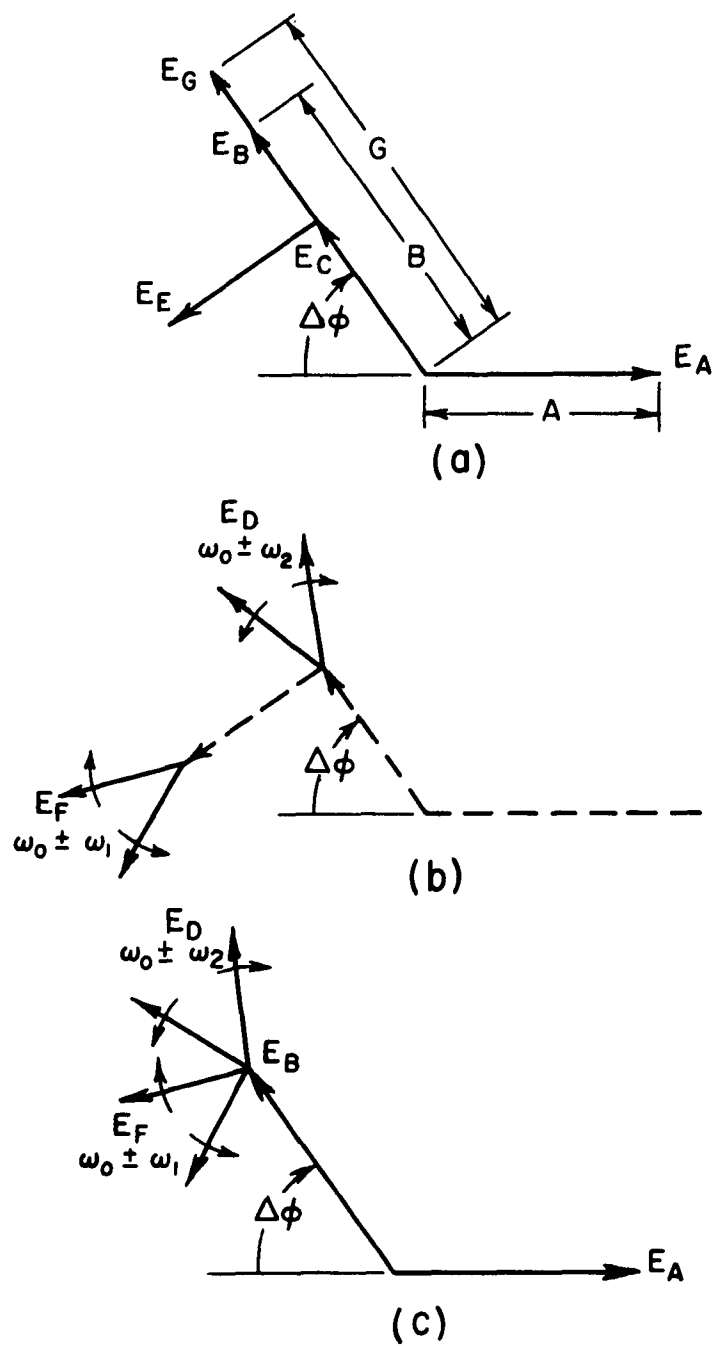nulling system.

16

Fig. 6. Phasor diagram of modulated information signals.

Fig. 6(a), the phase shifted carrier, $E_e$, is in quadrature with $E_b$, the processed interfering signal. The modulator output signal, $E_f$, is a double sideband, suppressed-carrier signal of frequencies of $f_o \pm f_1$. $E_f$ is illustrated in Fig. 6(b). When combined with $E_b$, the processes interfering signal, $E_f$, becomes phase modulation on the carrier $E_b$. The phase relationship between $E_f$ and $E_b$ is shown in the phasor diagram of Fig. 6(c).

As shown in the block diagram of Fig. 5, the balanced modulator I is parallel to balanced modulator II. Employing a modulation signal of audio frequency $f_2$, balanced modulator II produces sidebands which monitor the amplitude error B-A. The portion of $E_g$ introduced into balanced modulator II is identified as $E_c$. As indicated in Fig. 6(a), $E_c$ is kept in phase with $E_b$. The output, $E_d$, of balanced modulator II is a double sideband, suppressed-carrier signal of frequencies $f_o \pm f_2$. Figure 6(c) indicates the signal $E_d$ is in phase with the processed interfering signal $E_b$ and in quadrature with the signal $E_f$.

The composite signal from the nulling system, $E_d + E_f + E_b$, combines with $E_a$. The resulting signal $E_h$, at the input of the receiver may be expressed as

$$(14) \qquad E_h = B \cos \omega_0 t + m_2 \cos \omega_2 t \; \cos \omega_0 t$$

$$+ m_1 \cos \omega_1 t \cos(\omega_0 t + \pi/2)$$

$$+ A \cos(\omega_0 t - (\pi - \Delta\phi))$$

$$(15) \qquad = -(A \sin \Delta\phi + m_1 \cos \omega_1 t) \sin \omega_0 t$$

$$+ (B - A \cos \Delta\phi + m_2 \cos \omega_2 t) \cos \omega_0 t$$

where

$m_1$ = the signal strength of the phase information sidebands

$m_2$ = the signal strength of the amplitude information sidebands.

The information sidebands of Eq. (15) remain unsuppressed when the interfering signal is cancelled. These sidebands cannot cause cross-modulations, since they are limited to millivolts in strength. Yet, these sidebands must be several volts in strength at the servo-system input. The r.f. amplifier shown in the block diagram of Fig. 5 supplies a portion of the needed gain. The remainder of the amplification is provided by the audio amplifier.

Following r.f. amplification, $E_h$ is square-law detected. The output voltage of a square-law detector is

$$(16) \qquad e_{out} = K \, e_{in}^2 .$$

The audio output voltage, $e_{audio}$, from the square-law detector for input signal $E_h$ may be computed from equations (15) and (16), from which

19

(17) $$e_{audio} = K\left[\frac{B^2}{2} + \frac{A^2}{2} - 2AB \cos \Delta\phi\right.$$

$$+ A \sin \Delta\phi \; m_1 \cos \omega_1 t$$

$$+ (B - A \cos \Delta\phi) \; m_2 \cos \omega_2 t$$

$$\left. + \frac{m_1^2}{4} \cos 2\omega_1 t + \frac{m_2^2}{4} \cos 2\omega_2 t\right].$$

Envelope detection, a more commonly employed type of amplitude modulated signal detection, will not give the desired error signals. As indicated in Eq. (15), the error information is actually contained in the carriers and not in the sideband contribution to the envelope.

The only signal components of $e_{audio}$ in Eq. (17) at the frequencies $f_1$ and $f_2$ are the phase and amplitude error signals. Because these frequencies are different, each of the error signals can be separated from the other signal components of $e_{audio}$. The extraction of the error signals from $e_{audio}$ is achieved by synchronous detection. The amplified audio signal of Eq. (17) is fed into the parallel synchronous detectors I and II as shown in Fig. 5. The synchronous detectors I and II operate at frequencies $f_1$ and $f_2$ respectively. Each of the double-ended choppers, when used as a synchronous detector, provides an output voltage $e_{sync}(t)$, which is of the form

(18) $$e_{sync}(t) = 2e_{audio}(t)\left[\sum_{n=1}^{\infty} \frac{\sin \frac{n\pi}{2}}{\frac{n\pi}{2}} \cos n\omega_{chop} t\right]$$

where $\omega_{chop}$ = frequency of the chopper vibrating arm. The output

signals from the synchronous detectors are fed into low pass filters

to eliminate any remaining a.c. signals. The output d.c. error

voltage $e_{phase}$ of synchronous detector I is

(19) $\qquad e_{phase} = k_1 A \sin \Delta\phi$

where $k_1$ is a constant independent of A, B, and $\Delta\phi$. The d.c. output

voltage of synchronous detector II is

(20) $\qquad e_{amplitude} = k_2 (B-A \cos \Delta\phi),$

where $k_2$ is a constant independent of A, B, and $\Delta\phi$.

The phase error voltage, $e_{phase}$, indicates the true null

independent of the amplitudes A and B. In contrast, for non-zero

values of $\Delta\phi$, the amplitude error voltage, $e_{amp}$, indicates a false

null. However, as indicated by Eq. (20), the amplitude error voltage

approaches B-A for small values of $\Delta\phi$. Curves of the theoretical

error voltages, $e_{amp}$ and $e_{phase}$, appear in Fig. 7(a) and (b) as

functions of B-A and $\Delta\phi$.

D. Attainment of Null for an AM
   Interfering Signal

Because amplitude modulation is used extensively in shipboard

communications, a practical nulling system must be capable of

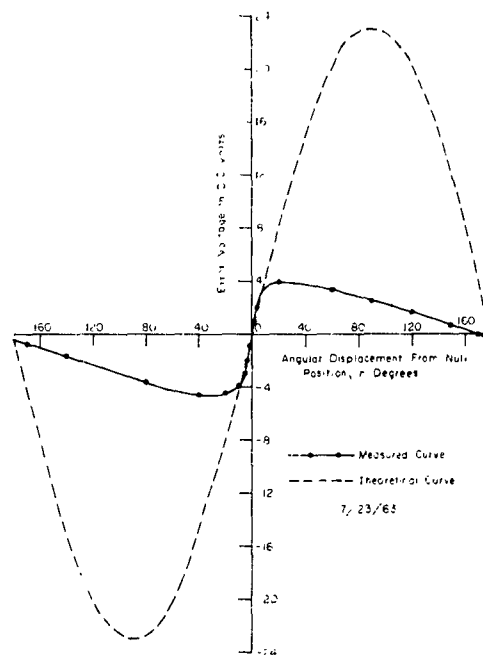suppressing an AM interfering signal. Section II B described the

21

Fig. 7(a). Phase system error voltage as a function of shaft displacement from null position.
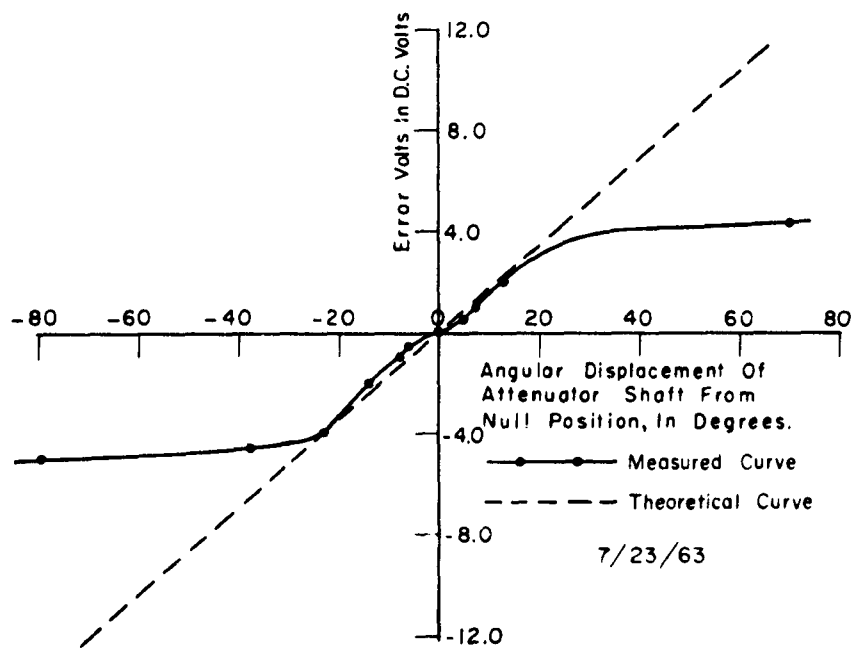


Fig. 7(b). Amplitude system error voltage as a function of attenuator shaft displacement from null position.

limited interference suppression at sideband frequencies for a cancellation system in which a delay line is simulated by a phase shifter. The depth of null is limited even though the system sustains a null at the interfering signal center frequency. If the modulation on the interfering signal obscures the error signals of an automatic nulling system, the depth of null will be further reduced. Therefore, an important factor in the practicality of an automatically controlled nulling system is that it be able to provide correct null information in the presence of modulation.

The origin of additional, unwanted signals at the error signal frequencies $f_1$ and $f_2$ will be investigated for an interfering signal with sinusoidal modulation. The interfering signal $E_{a_1}$ may be represented in standard notation as

$$(21) \qquad E_{a_1} = A_1(1 + m \cos \omega_m t) \cos \omega_0 t$$

where

     $m$ = index of modulation

     $\omega$ = $2\pi \times$ modulation frequency of 200 cps to 5 kcps

     $\omega_0 = 2\pi \times$ carrier frequency of 2 to 30 m.c.

The AM interfering signal is processed by the nulling system similarly to the c.w. signal as described in Section II C. The processed AM signal has additional modulation components generated

23

by the balanced modulators labeled I and II in Fig. 5. The receiver input signal $E_{h_1}$ for the AM signal case is similar to $E_h$ for the c.w. case and may be expressed as

(22)
$$E_{h_1} = B_1 (1 + m \cos \omega_m t) \cos \omega_o t$$
$$+ m_2 (1 + m \cos \omega_m t) \cos \omega_2 t \cos \omega_o t$$
$$+ m_1 (1 + m \cos \omega_m t) \cos \omega_1 t \cos(\omega_o t + \pi/2)$$
$$+ A_1 (1 + m \cos \omega_m t) \cos(\omega_o t - (\pi - \Delta\phi))$$

(23)
$$= -(A_1 \sin \Delta\phi + m_1 \cos \omega_1 t)(1 + m \cos \omega_m t) \sin \omega_o t$$
$$+ (B_1 - A_1 \cos \Delta\phi + m_2 \cos \omega_2 t)(1 + m \cos \omega_m t) \cos \omega_o t .$$

As in the c.w. case, the AM resultant signal at the receiver input, $E_{h_1}$, is r.f. amplified and square law detected. The square law detected signal $e_{audio_1}$ is

(24)
$$e_{audio_1} = K \left[ 1 + 2m \cos \omega_m t + \frac{m^2}{2} + \frac{m^2}{2} \cos 2\omega_m t \right]$$
$$\left[ \frac{B_1^2}{2} + \frac{A_1^2}{2} - 2A_1 B_1 \cos \Delta\phi + A_1 m_1 \sin \Delta\phi \cos \omega_1 t \right.$$
$$+ (B_1 - A_1 \cos \Delta\phi) m_2 \cos \omega_2 t + \frac{m_1^2}{4} \cos 2\omega_1 t$$
$$\left. + \frac{m_2^2}{4} \cos 2\omega_2 t \right] .$$

The term $m \cos \omega_m t$ is always less than one for properly modulated signals. Therefore, the factor in Eq. (24) resulting from

24

$(1 + m \cos \omega_m t)^2$ is always greater than zero. Consequently the error

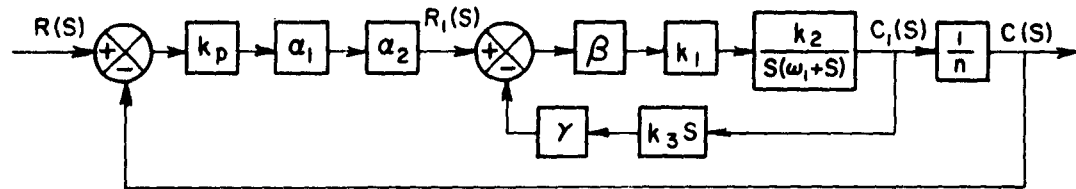signals will indicate the direction of the true null.

The recovery of the error signals at frequencies $f_1$ and $f_2$ is

still possible for the AM case as indicated by the presence of a

constant in the $(1 + m \cos \omega_m t)^2$ factor in Eq. (24). However, the

error signals may be obscured by the introduction of additional

signals at the frequencies $f_1$ and $f_2$. The additional audio signals

arise in the expansion of Eq. (24) which includes the multiplying

factors $\cos \omega_m t$ and $\cos 2\omega_m t$. An additional audio signal will be of

frequency $f_1$ when $\omega_m$ has the value $\frac{\omega_1}{2}$, $\frac{\omega_2 - \omega_1}{2}$, $\omega_1$, $\frac{3\omega_1}{2}$, $\frac{\omega_2 + \omega_1}{2}$, $2\omega_1 - \omega_2$,

$2\omega_1$, $2\omega_1 + \omega_2$, or $3\omega_1$. Likewise, interfering audio signals of fre-

quency $f_2$ are present when $\omega_m$ has the value $\frac{\omega_2}{2}$, $\frac{\omega_2 - \omega_1}{2}$, $\omega_2$, $\frac{3\omega_2}{2}$,

$\frac{\omega_2 + \omega_1}{2}$, $2\omega_2 - \omega_1$, $2\omega_2$, $2\omega_2 + \omega_1$, or $3\omega_2$.

Thus, the modulated signal obscures the error signals if it

contains audio frequencies less than or equal to $3f_2$, where $f_2$ is

assumed to be greater than $f_1$. To eliminate the possibility of addi-

tional signals at the error signal frequencies, the third harmonic of

$f_2$ must be at a lower frequency than the lowest modulating frequency.

A typical AM signal contains frequencies as low as 200 cps. Con-

sequently, the value of $f_2$ is restricted to 60 cps. The servo-controlled

nulling system will respond to suppress the carrier of an AM inter-

fering signal provided $f_1$ and $f_2$ are less than or equal to 60 cps.

25

E. Analysis of the Servo System

One of the factors which determine the effectiveness of the servo-controlled nulling system as an interference suppressor is the speed of response of the system. In the shipboard environment the time delay, $\tau$, between receiver and transmitter antennas and the interfering signal strength, k, will constantly vary about mean values. The minute variations in $\tau$ and k are due to antenna movement caused by wind and ship vibration. To provide continual cancellation, the nulling system must respond quickly, producing the corresponding changes of $\phi$ and $\alpha$ in the processed signal.

An expression for the speed of response of the system will be derived using servomechanism theory. The entire nulling system illustrated in Fig. 5 may be analyzed as two servo systems. The phase system is driven by an error voltage, A sin $\Delta\phi$. The amplitude system responds to the error voltage B-A cos $\Delta\phi$. For small values of $\Delta\phi$ the systems are independent; consequently, they may be analyzed separately. The phase and the amplitude systems may be represented by the same block diagram which appears in Fig. 8. The inner loop represents the rate generator feedback path. The outer loop provides a path for the correction caused by a change in the amplitude or the phase control shaft.

26

Definition of terms

$k_p$ = error gain
$k_1$ = gain of servo amplifier
$k_3$ = gain of rate generator
$\alpha_1$ = conversion of voltage from d.c. to a.c. fundamental 400 cps
$\alpha_2$ = attenuation of summing point
$\beta$ = attenuation due to finite input impedance of filter
$\gamma$ = attenuation of summing point on fed-back signal
$k_2$ = gain constant of motor
$\omega_1$ = corner frequency of motor
$\dfrac{1}{n}$ = gear ratio

Fig. 8. Block diagram for phase or amplitude
servo system.

The transfer function for the servomotor represented in Fig. 8

is $\dfrac{k_2}{s(s+\omega_1)}$. The motor transfer function may be developed from the

torque balance equation which is

$$(25) \qquad k_2' \, v_c(t) = \frac{J \, d^2 c_2(t)}{dt^2} + \frac{B \, dc_2(t)}{dt}$$

where

$v_c(t)$ = control voltage input to the motor

$k_2'$ = a constant which linearly relates the control

voltage to the torque developed by motor

$c_2(t)$ = the motor shaft position

J = intertia of motor in kg.-m$^2$

B = friction of motor, gears, and load in

(new. - sec.)/rad.

Converted to Laplace transform notation, Eq. (25) becomes

$$(26) \qquad k_2' v_c(s) = (Js^2 + Bs) C_2(s)$$

$$(27) \qquad \frac{C_1(s)}{v_c(s)} = \frac{k_2'/J}{s(s+B/J)}$$

$$(28) \qquad \frac{C_1(s)}{v_c(s)} = \frac{k_2}{s(s+\omega_1)}$$

where

$$k_2 = k_2'/J$$

$$\omega_1 = B/J \ .$$

The transfer function $C_1(s)/R_1(s)$ for the ᵢ ner loop of the model in Fig. 8 may be written as

$$(29) \qquad \frac{C_1(s)}{R_1(s)} = \frac{G(s)}{1 + G(s)H(s)}$$

where

G(s) = forward path transfer function

H(s) = feedback path transfer function.

28

In reference to Fig. 8, the transfer function $\frac{C_1(s)}{R_1(s)}$ may be written

$$(30) \qquad \frac{C_1(s)}{R_1(s)} = \frac{\beta k_1 k_2}{s(s + \omega_1 + \beta \gamma k_1 k_2 k_3)} = G_1(s) .$$

The term $\omega_1$, the damping term, is a constant for the motor. Upon addition of rate generator feedback, the effective value of $\omega_1$ and hence, the damping is increased. Since the damping term is inversely proportional to the system time constant, increased damping decreases the response time.

The transfer function for the entire system may be found by replacing the inner loop with an effective forward path transfer function $G_1(s)$. According to Eq. (29) and Fig. 8, the transfer function for the system is

$$(31) \qquad \frac{C(s)}{R(s)} = \frac{\alpha_1 \alpha_2 k_p G_1(s)/n}{1 + \alpha_1 \alpha_2 k_p G_1(s)/n}$$

$$(32) \qquad \frac{C(s)}{R(s)} = \frac{\alpha_1 \alpha_2 \beta k_1 k_2 k_p/n}{s^2 + s(\omega_1 + \beta \gamma k_1 k_2 k_3) + \alpha_1 \alpha_2 \beta k_1 k_2 k_p/n}$$

$$(33) \qquad \frac{C(s)}{R(s)} = \frac{\omega_n^2}{s^2 + s 2\zeta \omega_n + \omega_n^2}$$

where

$$(34) \qquad \omega_n^2 = \alpha_1 \alpha_2 \beta k_1 k_2 k_p/n$$

$$(35) \qquad 2\zeta \omega_n = \omega_1 + \beta \gamma k_1 k_2 k_3 .$$

The driving function r(t) represents the desired phase or amplitude of the interfering signal fed through the processing path. In general, the driving function is non-deterministic. Therefore, necessary information about the system performance must be obtained by examining the system response to a step input function. The solution to Eq. (35) is obtained by setting $R(s) = \frac{1}{s}$ and taking the inverse Laplace transform. The resulting solution for c(t), the position of the control shaft, is

$$(36) \qquad c(t) = 1 - e^{-\zeta\omega_n t} \sin\left[(\sqrt{1-\zeta^2})\,\omega_n t + \tan^{-1}\left(\frac{\sqrt{1-\zeta^2}}{\zeta}\right)\right].$$

Parameters providing a figure of merit for the system may be determined from Eq. (36). The effective system time constant may be defined as

$$(37) \qquad \tau = \frac{1}{\zeta\omega_n}.$$

Another important system parameter, the actual frequency of system oscillation, is

$$(38) \qquad \omega = \omega_n(\sqrt{1-\zeta^2}).$$

The response time or speed of response of a system is defined as the time corresponding to four time constants,[8] or

$$(39) \qquad t_r = 4\tau.$$

The constants needed to evaluate $\zeta$ and $\omega_n$ are defined in Fig. 8.

The experimental values of the constants are listed in Table 1 in

Section III C. The calculated values of $\omega_n$ and $\zeta$ were used to compute

the system parameters $\omega$ and $t_r$ for the phase and the amplitude sys-

tems. The computed values of $\omega$ and $t_r$ appear in Table 2 in Section

III C.

In order to facilitate the analysis of the servo system, the

time constant added by the band pass filter was not considered. As

may be illustrated by root-locus plots of 2nd and 3rd order systems,

the analysis employed in this section produces results which approxi-

mate the actual system only for small values of open-loop gain.

# CHAPTER III
## EXPERIMENTATION

A. **Description of the Nulling System**
   **Circuitry**

The theory developed for the servo-controlled nulling system

illustrated in the block diagram of Fig. 5 was verified experimentally.

As the purpose of the study was to investigate the feasibility of the

nulling system concept, no attempt was made to develop a system

capable of handling large interfering signals. The constructed system

cancelled a 4.5 mc. c.w. signal for signal strengths ranging from

0.1 to 0.7 volts peak to peak. The experimental model is pictured

in the photograph of Fig. 9. Circuit diagrams of the modular com-

ponents of the nulling system appear in Figs. 10, 11, 12, and 13.

The important portions of the circuitry will be discussed in some

detail.

The phase shifter illustrated in Fig. 10 is a phase-shifting

capacitor.[9] The angular position of the capacitor shaft determines

the amount of phase shift experienced by the output voltage. To

provide an output phase shift which may be varied from $0^{\circ}$ to $360^{\circ}$,

the phase shifter must be excited by four voltages in quadrature and

of equal amplitude. The necessary phase shifter excitation circuitry

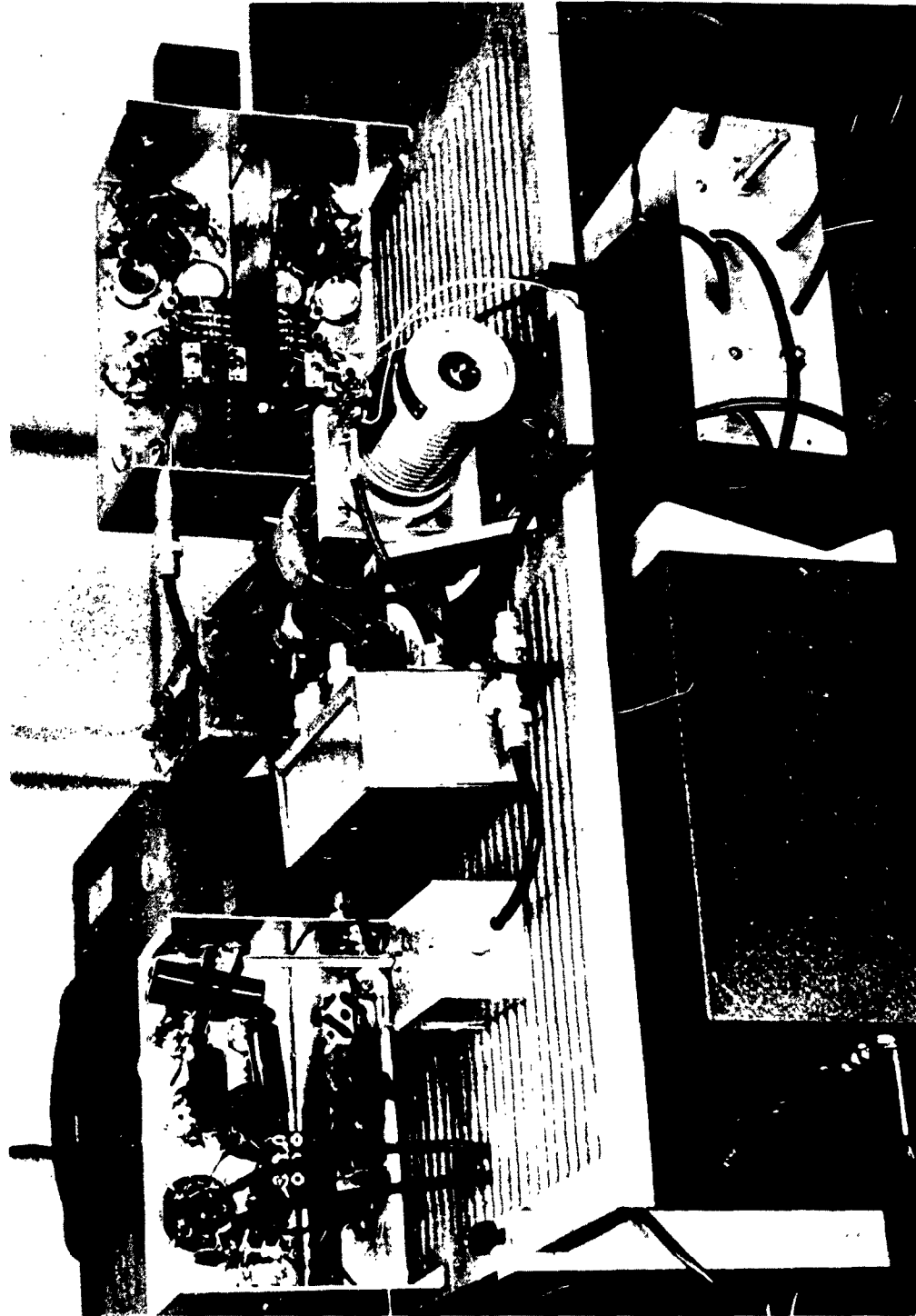is also illustrated in the circuit diagram. Since the output impedance

32

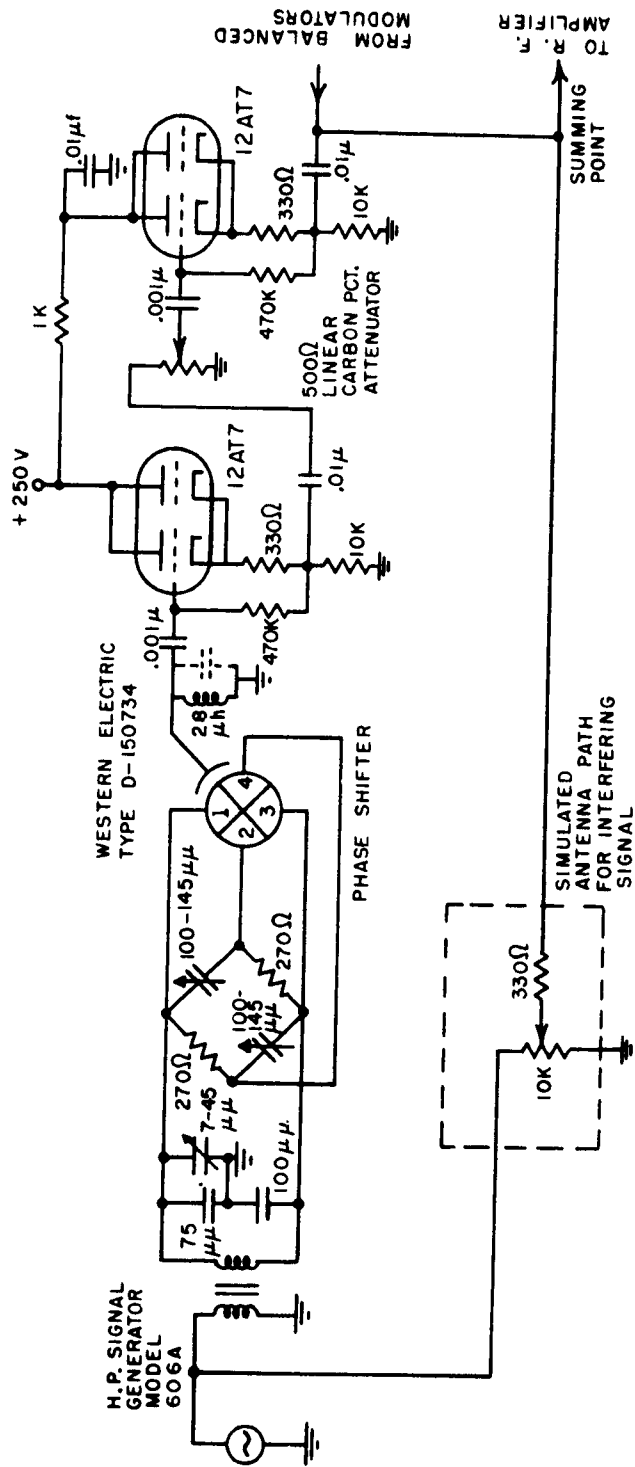Fig. 9. Photograph of experimental model of servo-controlled, nulling system.

Fig. 10. Circuit diagram of fed-through and simulated radiation paths.

34

of the phase shifter at 4.5 mc was quite high, a cathode follower was used to lower the impedance level without creating a significant reduction in voltage.

According to the assumptions stated in Section II B, the phase shifted output, $\phi$, is constant for a limited range of input frequencies. Investigation of the capacitor output phase shift for frequencies higher than the design center frequency indicates that the phase shift $\phi$ actually decreases slightly with increasing frequency. However, for an input frequency range of 40 kc about the center frequency 4.5 mc the phase decrease with increasing frequency was negligible compared to the phase slopes resulting from practical values of $\Delta t$.

The circuitry for the attenuator $\alpha$ in Fig. 5 is illustrated in Fig. 10. A linear carbon potentiometer was used as an attenuator to control the output amplitude of the signal fed through the processing path. The cathode follower at the attenuator output prevented attenuator loading. Because the attenuator output was unloaded, the attenuator shaft deviation from the null position was directly proportional to B-A.

The signal processing path and the external path combine at the summing point illustrated in the circuit diagram of Fig. 10. The signal from the external path enters the summing point through a 330 ohm resistor. The actual signal summation is achieved at the

low output impedance of the attenuator cathode follower. Signal summation employing summing resistors is a lossy method, and therefore not adaptable to high power levels. In a practical, high power nulling system, summation of the external and processed signal would be achieved through the use of a diplexer such as a hybrid transformer.[10]

The circuit diagrams of the balanced modulators appear in Fig. 11. As described in Section II C, the function of the modulators. is to provide error information sidebands. Balanced modulators are required to suppress the carrier frequency signal. The balanced modulators constructed suppressed the residual carriers 30 db below the sideband signal level of 5 mv peak to peak. The modulating signal frequencies used were $f_1$ = 400 cps and $f_2$ = 700 cps. These frequencies were chosen arbitrarily and could have been much lower. The required phasing in the balanced modulator circuits was obtained principally through the use of center tapped transformers with R-C split loads. This method proved to be inefficient at r.f. frequencies because of the low impedance level of the circuitry. Additional phase-shift was obtained, as required, by using L-C tuned circuits.

The combined signal from the summing point enters the r.f. amplifier included in the circuitry of Fig. 12. The tuned plate load of the pentode tube and the tuned output transformer provide

36

Fig. 11. Circuit diagram of balanced modulators.

preselection to reduce the effect upon the nulling system of other, un-cancelled interfering signals. Another function of the r.f. amplifier, is to provide a portion of the needed error gain. The cathode follower used in the r.f. amplifier provides a low impedance source which is required for the square-law detector circuit. The square-law detector is a microwave diode..

The filter system for achieving error signal separation is also illustrated in Fig. 12. The choppers provide synchronous detection at each of the information frequencies $f_1$ and $f_2$. The remaining a.c. signals are eliminated by the low pass filter which has a cut-off frequency of 60 cps. The desired d.c. error voltages are modulated at 400 cps, the excitation frequency of the servo motors, by the chopper modulator.

The 400 cps square wave error voltages enter the inner loop servo systems illustrated in Fig. 13. The inner loop phase and amplitude servo system circuits are similar, differing only in component values. A high impedance potentiometer is used as a summation device to combine the signals representing the actual position of the motor shaft and the desired position. The signal from the summing device is filtered by an L-C resonant circuit of 20 cps bandwidth to reduce 60 cps pick up. The error signal is amplifier by a Heathkit audio amplifier and applied to the control voltage winding of the servo motor.
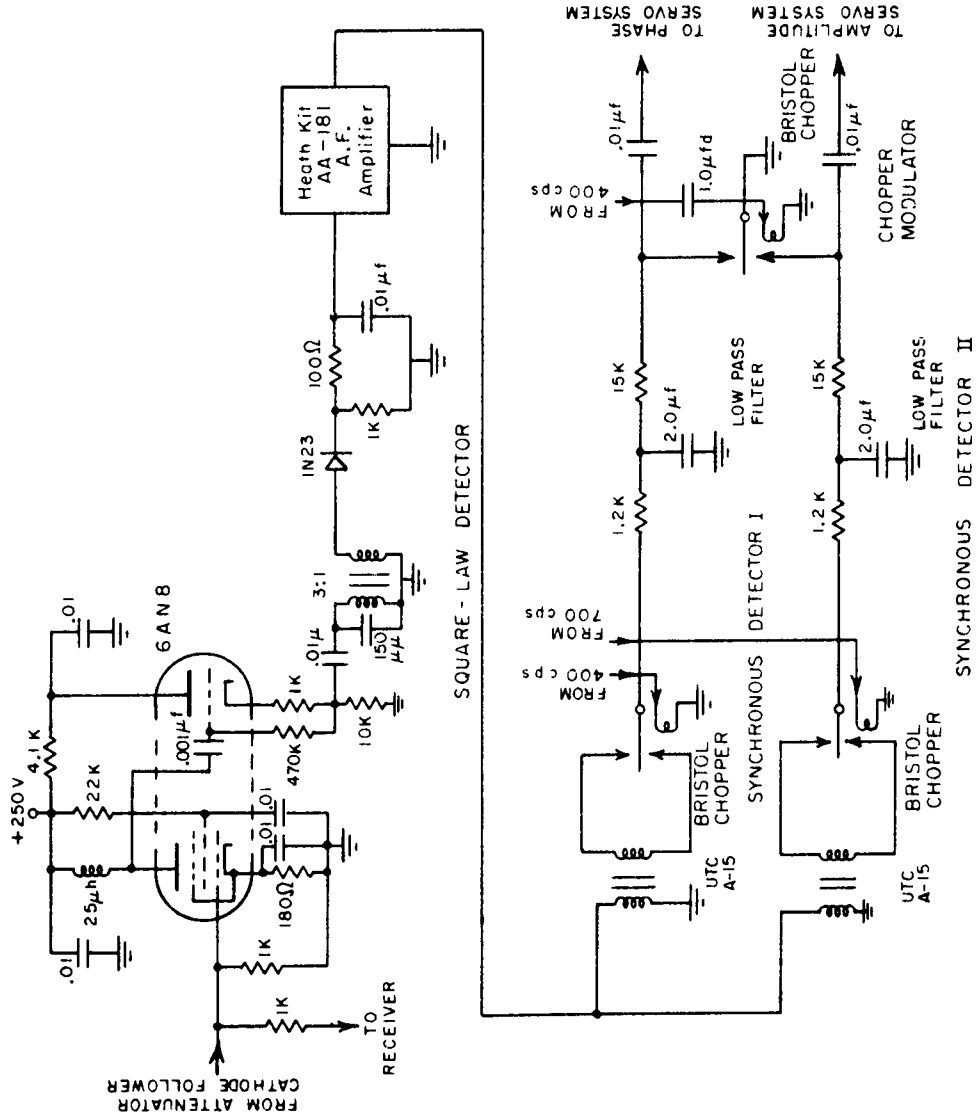
38

Fig. 12. Circuit diagram of r.f. amplifier and detector circuits.
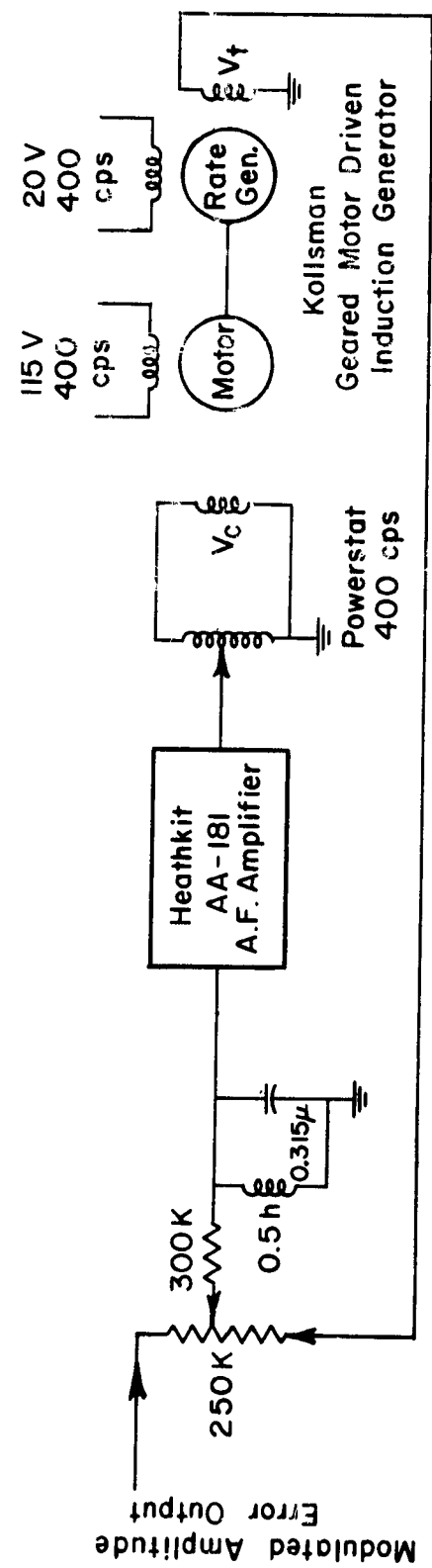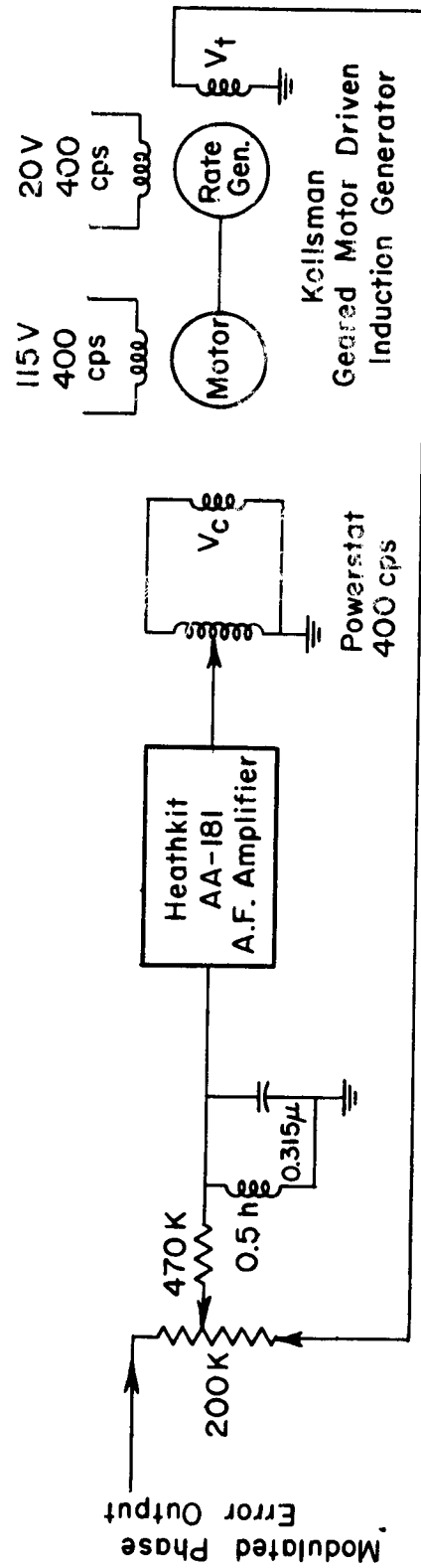
39

Fig. 13. Circuit diagram of phase and amplitude servo-systems.

40

B. Measurement of d.c. Error Voltages

In order to verify the predicted error voltages and to determine the error gain constant, the d.c. error voltages were measured. The phase error voltage was measured at the phase system low pass filter illustrated in Fig. 12. The error voltage was recorded as a function of the phase shifting capacitor shaft angular position with the amplitude error set equal to zero. Since a close correspondence existed between electrical output phase and shaft angular position, the phase deviation, $\Delta\phi$, from null position could be determined.

The measurement procedure was repeated on the amplitude system. With the phase error equal to zero, the amplitude error voltage was recorded as a function of attenuator shaft angular position. The attenuator was linear; consequently, the shaft deviation from null position was proportional to the amplitude difference, B-A.

Curves of the measured phase and amplitude error voltages appear in Fig. 7. The curves may be compared with the corresponding theoretical curves predicted in Section II C. The measured phase error curve has a sinusoidal form. At small deviations the phase error voltage closely approximates the sine curve. However, at larger values of $\Delta\phi$, the phase error voltage is heavily limited. The voltage returns to zero near $\pm 180°$. The measured amplitude error curve is similar to the predicted linear curve. Although

heavily limited, the amplitude error voltage does not approach zero

for larger amounts of deviation from the null position. The measured

amplitude error curve has region of reduced slope near the null

position.

The limiting present in both measured curves is a result of

saturation in the square-law detector. Measurements on the square-

law detector indicate that it is no longer square-law for input signals

in excess of 1.0 volt peak-to-peak. Since the r.f. amplifier pre-

ceeding the detector has a gain of 5, the error gain is limited when

the resultant signal at the summing point exceeds 0.2 volts. Thus,

for an interfering signal of 0.6 volts, the square law detector may

be calculated to limit the error information for $\Delta\phi$ exceeding $45^\circ$.

The error gain $k_p$ may be determined from the measured curves

of Figs. 7(a) and 7(b). By linear approximation of the error curve

near the null position, the error curve slopes may be measured in

units of volts d.c./radian. The slope of the error curve is the error

gain, $k_p$, as defined in Fig. 8. The measured values of the phase

and the amplitude error gains appear in Table 1 in Section III C.

C.  Measurement of the Servo System Response

The actual resonant frequency, $\omega$, and the response time, $t_r$,

were measured for the experimental servo-controlled nulling system.

The measurements were made with the phase and the amplitude servo

42

motors in operation. While in operation, the phase system motor was

manually forced from the angular null position to create a unit step

error function. The phase system response to the step function error

was obtained by observing the input control voltage to the phase sys-

tem servo motor after the shaft was released. A photograph of the

phase system response appears in Fig. 14. The response time was

determined by measuring the interval between the time the shaft was

released and the time at which the response had decayed to zero.

The actual frequency of oscillation was computed from the period of

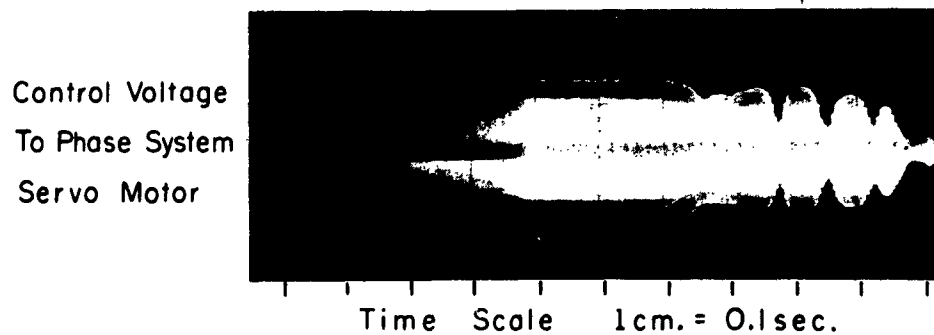oscillation of the response wave form.



Fig. 14. Control voltage response of phase
system servo motor for a unit
step function error.

The measurements were repeated to obtain amplitude system response. To obtain the amplitude response, the amplitude control voltage was observed following release of the displaced attenuator shaft. Photographs of the amplitude servo motor control voltage response were taken for displacements of attenuator shaft position. The response of the combined system was measured by displacing both the phase and amplitude control shafts from null position. The measured value for the combined system response time is 0.60 sec. The averages of the measured values of $t_r$ and $\omega$ for the phase and the amplitude system are listed in Table 2 together with the values computed from the formulas derived in Section II E.

TABLE 1

Constants for the phase and amplitude servo systems

| | Phase System | Amplitude System |
|---|---|---|
| $k_p$ | 34.2 v d.c./rad. | 6.0 v d.c./rad |
| $k_1$ | 10,100 | 10,400 |
| $k_3$ | $1 \times 10^{-3}$ vrms/rad/sec | $1 \times 10^{-3}$ vrms/rad/sec |
| $\alpha_1$ | 0.225 vrms/vdc | 0.225 vrms/vdc |
| $\beta$ | 0.0425 | 0.061 |
| $\gamma$ | 0.28 | 0.185 |
| n | 50 | 100 |
| $\alpha_2$ | .667 | 0.776 |
| | | |
| $k_2$ | 75.5 | 75.5 |
| $\omega_1$ | 7.3 | 7.3 |

## TABLE 2

### Measured and computed values of servo system response

|  | Computed value | Measured value |
|---|---|---|
| $f_{phase}$ | 9.1 cps | 7.2 cps |
| $f_{amp}$ | 3.3 cps | 5.0 cps |
| $t_{r\ phase}$ | 0.49 sec | 0.40 sec |
| $t_{r\ amp}$ | 0.50 sec | 0.55 sec |

The oscilloscope photograph of the phase system response, Fig. 14, indicates an initially overdamped system. As the response decays toward zero the damping decreases and the response becomes oscillatory. The change in response is caused by the behavior of error gain, $k_p$, as displacement from the null is increased. The slope of the phase error curve in Fig. 7(a) and consequently, $k_p$ diminish rapidly when the displacement angle exceeds $20^\circ$. As indicated by Eq. (34), $\omega_n$ decreases as $k_p$ is diminished. The term $2\zeta\omega_n$ is a constant which is independent of $k_p$ according to Eq. (35). Therefore, as $\omega_n$ decreases, $\zeta$ must increase causing an overdamped condition. As the system heads toward the null position, the increasing $k_p$ increases $\omega_n$. At the same time $\zeta$, the damping ratio, must decrease, causing the oscillations to become more pronounced. The change from overdamping to underdamping and the corresponding increase in $\omega$ are indicated in the oscilloscope photograph of Fig. 14.

## D. Depth of Null for a 4.5 mc Signal

With the nulling system servo-controlled, sustained depths of null were achieved for an interfering 4.5 mc c.w. signal. The null depths were measured and recorded as a function of the signal strength of the interfering signal. As illustrated in Fig. 15, the null measurement system included a Hewlett-Packard r.f. attenuator and a Collins 75 S-3 receiver operating in the narrow band, c.w. mode of reception.
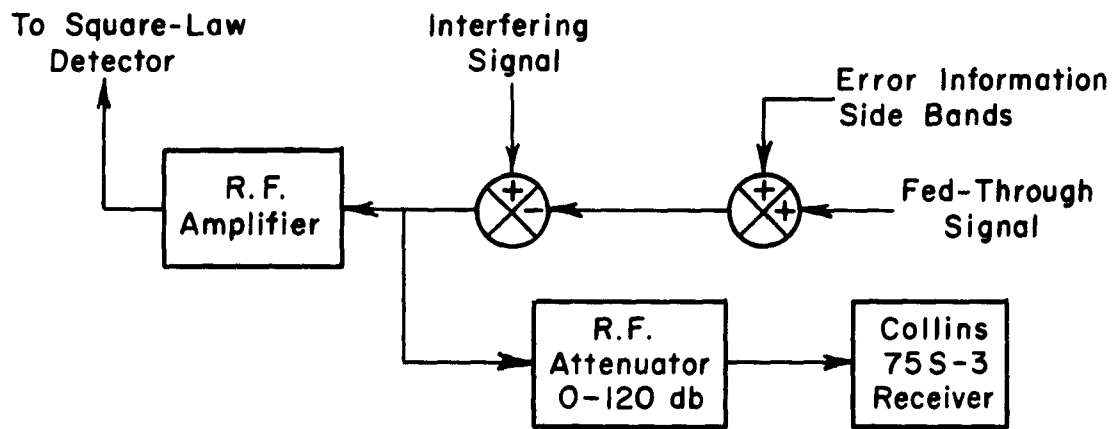


Fig. 15. Block diagram of null measurement system.

The measurement procedure was initiated by recording the attenuator setting in db's and the dial reading on the S meter of the receiver when the interfering signal was nulled. After the

servo-amplifiers were disconnected, the phase shifter was rotated

manually 180° to the anti-null. The amplitude control shaft was not

changed from the null position. With the system at the anti-null,

the amount of attenuation needed to return the S meter dial to its

original position was recorded. To obtain the true depth of null,

6 db was subtracted from the difference of the two readings.

Twice the nulled voltage, or an additional 6 db of signal power

is present at the anti-null, where the signals are added in phase.

The results of these measurements are graphically illustrated

in the curves of Fig. 16. In general, the depth of null for all three

curves tends to diminish as the nulling signal decreases in size.

The tendency is caused by the decrease in error gain. The gains

of both external loops in the servo-systems are directly proportional

to A, the strength of the interfering signal. With the gain of the

servo-system reduced, its ability to respond to small displace-

ments from the null is also diminished. The loss of null depth

with smaller signals could be eliminated with proper gain com-

pensation in the servo system.

In measuring the null depths, steady state error was noticed.

By adding manual torque to the shafts of the nulled systems, a null

in excess of 25 db deeper, or -75 db, could be reached. In one of

the curves, identified by the key in Fig. 16, the steady state error
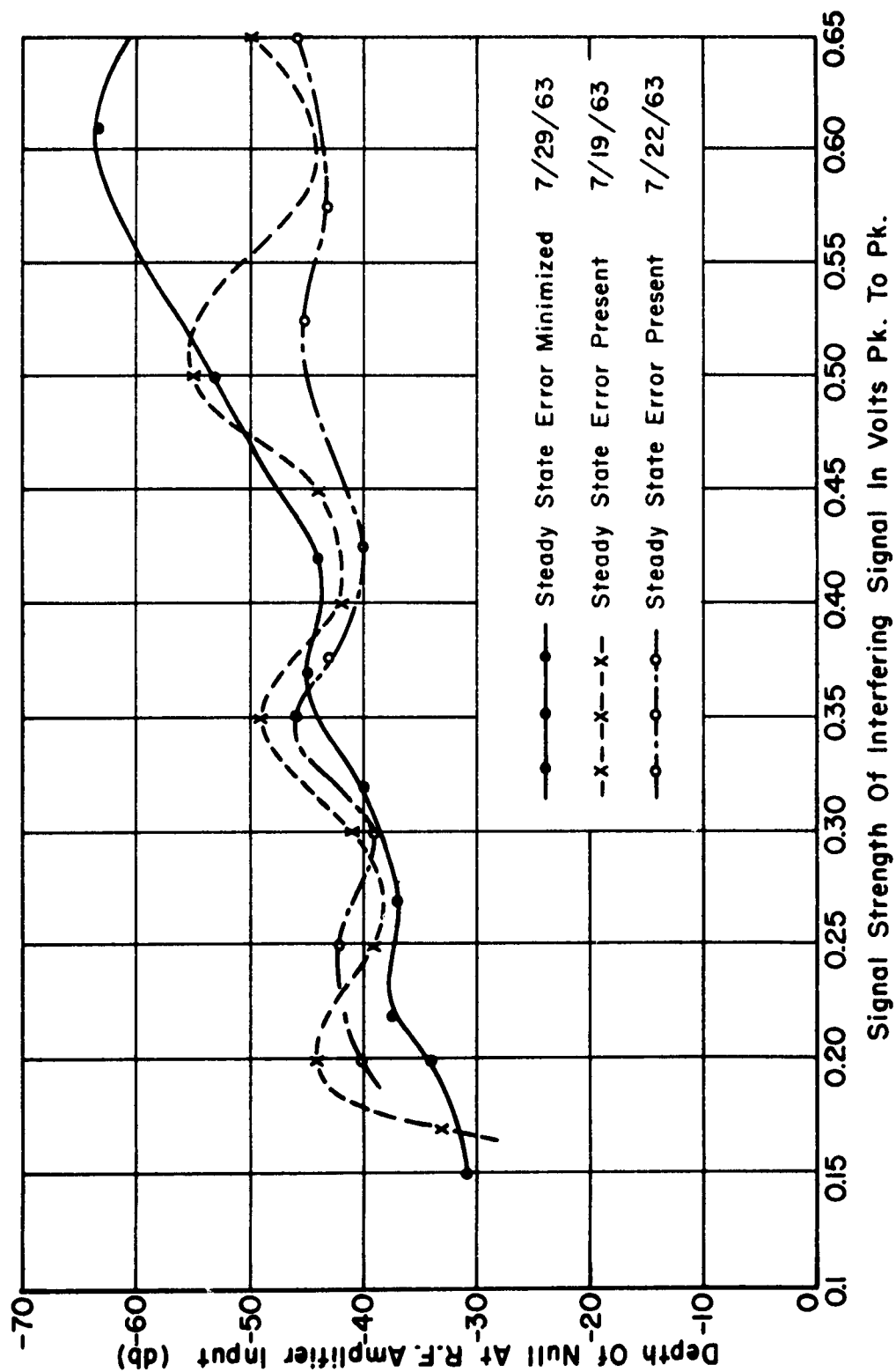
Fig. 16.  Depth of null at r.f. amplifier input as a function of interfering signal strength.

was minimized at 0.61 volts by introducing correctional d.c. voltage of the proper polarity following the synchronous detector. While the correction produced a -64 db null at 0.61 volts, the depth of null for other input signal strength was decreased.

Another salient feature of the two uncompensated curves is the sinusoidal variation of depth of null as a function of signal strength. The sinusoidal variation in all three of the curves appears correlated. The nulls recorded on the graph are averages of several readings. The individual measurements sometimes varied as much as 10 db between consecutive measurements at the same signal strength. This variation is thought to be the effect of an area of reduced gain near the null position in the amplitude system transfer function illustrated by the measured curve in Fig. 7(b). The specific cause of the correlated sinusoidal dependence upon signal strength could not be located.

Although the experimental system was not designed to null an amplitude modulated signal, an AM signal with 1000 cps sinusoidal modulation was fed into the nulling system. As expected, the second harmonic of the higher modulating frequency, 700 cps, multiplied with the 1000 cps signal produced a difference frequency of 400 cps. The difference frequency signal overloaded the servo-amplifier of the phase system operating at 400 cps. Overloaded with interference from the modulated signal, the system was unable to reach the null position.

49

To eliminate the spurious response of the servo system caused by the difference frequency, the amplitude system modulation frequency $f_2$ was lowered from 700 cps to 250 cps. With the lowered value of $f_2$, the system handled the 5% modulated signal producing a null of -45 db in a response time of several seconds. The effect of larger percentages of modulation increased the response time, but did not significantly affect the depth of null at the carrier frequency. The increased response time was attributed to audio amplifier saturation. The saturation was caused by the relatively large signal strength at the 1000 cps modulation frequency which is present at the square-law detector output when the signal is not nulled.

# CHAPTER IV
## SUMMARY

A. Conclusions

Nulls in c.w. interfering signals of 45 db or greater depth were achieved with the present experimental model. Further effort to reduce the steady state phase and amplitude errors should increase the null depth considerably.

No severe limitations exist that would prevent operation of the servo-controlled nulling system at high power levels of interfering signal. Circuit alterations would include a linear amplifier in the fed-through path following the phase shifter and attenuator. The addition of gain in the fed-through path would have the advantage of requiring less power from the interfering signal to cancel the signal on the receiver antenna. An additional servo system would be needed to control a protective attenuator preceding the r.f. amplifier.

The servo-controlled nulling system can be expected to null an interfering AM signal. The depth of null at the sideband frequencies will depend on the amount of time delay which must be approximated by the phase shifter.

Because of its compatibility with high power levels of signal and automatic response to the amplitude and the phase variations

of the interfering signal, the servo-controlled nulling system presents

a feasible solution to the shipboard interference problem.

## B.  Recommendations for Further Study

In order to ascertain the practicality of the nulling system, in-

vestigation must be extended.  A study of system design for simul-

taneously nulling signals from several interfering transmitters is

an important criterion of system practicality.  Nulling system

alterations needed to reduce interference from transmitters with

other types of modulation, such as single sideband, , should also be

considered.  Finally, experimentation should be extended to the

operation of a nulling system capable of cancelling signals of high

power levels under shipboard conditions.

# FOOTNOTES

[1] E. W. Pappenfus, "A Discussion of Receiver Performance," QST, (January 1955), p. 25.

[2] E. K. Sandeman, Radio Engineering, Vol. II, (London, 1953), p. 31.

[3] Pappenfus, op. cit., p. 27.

[4] E. A. Pappenfus, "Recent Trends in Receiver Front End Design," QST, (June, 1962), p. 17.

[5] Study Program Related to Shipboard Antenna System Environment, Ohio State University Antenna Laboratory Report 1522-3, (Columbus, June 1963).

[6] W. B. Warren, Jr., Communication Interference Reduction Study, (Atlanta, 1962).

[7] J. E. Trott, Monthly Progress Report to U. S. Navy Electronics Laboratory, (Springfield, Va., 1963).

[8] G. J. Thayler, Elements of Servomechanism in Theory, (New York, 1955), p. 17.

[9] E. A. Holmes, "Special Variable Condensers," Components Handbook, (New York, 1949), p. 288.

[10] L. Gray, Radio Transmitters, (New York, 1961), p. 299.

# BIBLIOGRAPHY

Andrade, E.A., "Recent Trends in Receiver Front End Design,"
    QST, Vol 46, June, 1962.

Gray, L. and Graham, R., Radio Transmitters, New York:
    McGraw-Hill, 1961.

Holmes, E.A., "Special Variable Condensors," Components
    Handbook, Radiation Laboratory Series, Vol. 17,
    Edited by John F. Blackburn, New York: McGraw-Hill,
    1949.

Pappenfus, E.W., "A Discussion of Receiver Performance,"
    QST, Vol 39, January,1955.

Sandeman, E.K., Radio Engineering, Vol II, 2nd ed., London:
    Chapman and Hall, 1953.

Study Program Related to Shipboard Antenna System Environment,
    Interim Engineering Report 1522-3, Antenna Laboratory,
    The Ohio State University Research Foundation, Columbus,
    Ohio: The Ohio State University, June 1, 1963.

Thaler, George J., Elements of Servomechanism Theory, New York:
    McGraw-Hill, 1955

Trott, John E., MonthlyProgress Report to U.S. Navy Electronics
    Laboratory, Springfield, Virginia: Scanwell Laboratories;
    June 4, 1963.

Warren, W.B., Jr., Communications Interference Reduction Study,
    AD-298 118, Final Report Project No. A-525, Engineering
    Experiment Station, Atlanta: Georgia Institute of Technology,
    December 3, 1962.